Absorption Properties of Metal–Semiconductor Hybrid Nanoparticles

Ehud Shaviv,[†,#] Olaf Schubert,[‡,△,#] Marcelo Alves-Santos,[§] Guido Goldoni,[§,⊥] Rosa Di Felice,[§] Fabrice Vallée,[∥] Natalia Del Fatti,[∥] Uri Banin,[†] and Carsten Sönnichsen[‡,*]

[†]Institute of Chemistry and the Center for Nanoscience & Nanotechnology, The Hebrew University of Jerusalem, Jerusalem 91904, Israel, [‡]Institute of Physical Chemistry, University of Mainz, Jakob-Welder-Weg 11, 55128 Mainz, Germany, [§]CNR Institute of Nanoscience, S3 Center, Via Campi 213/A, 41125 Modena, Italy, [⊥]Dipartimento di Fisica, Università di Modena e Reggio Emilia, Via Campi 213/A, 41125, Modena, Italy, and [∥]FemtoNanoOptics Group, LASIM, CNRS and Université Lyon 1, 43 Boulevard du 11 Novembre, F-69622 Villeurbanne, France. [#]Contributed equally. [△]Present address: Department of Physics, University of Regensburg, Universitätsstrasse 31, 93053 Regensburg, Germany.

ABSTRACT The optical response of hybrid metal–semiconductor nanoparticles exhibits different behaviors due to the proximity between the disparate materials. For some hybrid systems, such as CdS–Au matchstick-shaped hybrids, the particles essentially retain the optical properties of their original components, with minor changes. Other systems, such as CdSe–Au dumbbell-shaped nanoparticles, exhibit significant change in the optical properties due to strong coupling between the two materials. Here, we study the absorption of these hybrids by comparing experimental results with simulations using the discrete dipole approximation method (DDA) employing dielectric functions of the bare components as inputs. For CdS–Au nanoparticles, the DDA simulation provides insights on the gold tip shape and its interface with the semiconductor, information that is difficult to acquire by experimental means alone. Furthermore, the qualitative agreement between DDA simulations and experimental data for CdS–Au implies that most effects influencing the absorption of this hybrid system are well described by local dielectric functions obtained separately for bare gold and CdS nanoparticles. For dumbbell shaped CdSe–Au, we find a shortcoming of the electrodynamic model, as it does not predict the "washing out" of the optical features of the semiconductor and the metal observed experimentally. The difference between experiment and theory is ascribed to strong interaction of the metal and semiconductor excitations, which spectrally overlap in the CdSe case. The present study exemplifies the employment of theoretical approaches used to describe the optical properties of semiconductors and metal nanoparticles, to achieve better understanding of the behavior of metal–semiconductor hybrid nanoparticles.

KEYWORDS: plasmon · exciton · hybrid nanoparticles · Janus particles · DDA · absorption

Recently, the wet chemical synthesis of binary hybrid nanocrystals with controlled topologies, sometimes termed Janus particles,[1–5] has become feasible. Examples include core–shell semiconductor quantum dots,[6,7] linear and branched heterostructures comprised of two semiconductors,[8,9] magnetic-functionalized semiconductor nanorods,[10,11] and metal-tipped semiconductor nanorods and tetrapods.[1,3,12–17]

Metal–semiconductor hybrid nanoparticles are promising candidates for applications in solar energy conversion,[18] photocatalysis,[19,20] and electronic devices.[21] The nanoscopic dimensions of their components, namely, the semiconductor and the metal, result in size- and shape-dependent electronic and optical properties. These mainly result from quantum confinement[22] in the semiconducting part ("exciton") and the dielectric confinement ("surface plasmon") in the metal part, leading to a very high polarizability at the plasmon frequency.[23] Metal–semiconductor hybrids often exhibit markedly different properties than the individual components, thereby providing a powerful strategy for altering the properties of nanoparticles. For example, previous studies of semiconductor nanocrystals coupled to metals have exemplified the existence of a plasmonic "antenna effect", leading to amplified excitation or increased radiative decay rate of excitons in the semiconductor.[24–27] Coherent and incoherent interactions between the metal and the semiconductor may lead to broadening and shifting of the excitonic resonance and strong nonlinear effects.[28] Other studies have shown that charges generated by the optical excitation of the semiconductor domain can be transferred efficiently to the metal part, shifting the plasmon frequency[29–32] and/or promoting redox reactions.[19,31–35] The gold tips grown on semiconductor nanorods can also serve as anchoring points for self-assembly to create elaborate superstructures.[1,36,37] Moreover, the gold tips can serve as efficient contact points to external electrical circuits.[21]

Advances in the synthesis of binary hybrid systems allow a good degree of control on the composition and final shape of metal–semiconductor hybrid structures. For

* Address correspondence to soennichsen@uni-mainz.de.

Received for review February 16, 2011 and accepted May 31, 2011.

Published online June 07, 2011
10.1021/nn200645h

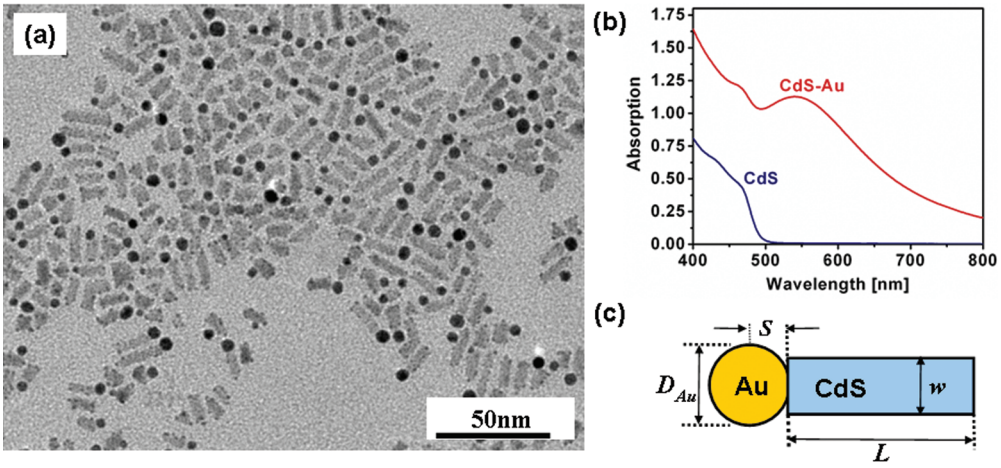

Figure 1. (a) TEM image of the CdS−Au matchstick-shaped sample used for the comparison of the experimentally measured absorption with DDA simulations. The mean CdS segment size is 14 nm × 5.3 nm. The average gold tip size is 6 nm. (b) The measured absorption spectra: template CdS nanorods sample (blue curve) CdS−Au sample after gold growth (red curve). (c) Schematic drawing of the geometry of the CdS−Au hybrid used for the DDA simulations. The following values were used for the simulations: D_{Au} =6 nm, L = 14 nm, w = 5.3 nm. The parameter S, which describes the offset between the center of the gold domain and the edge of the semiconductor cylinder, was set to S = 3 or S = 1.5 nm for a sphere- and half-sphere-shaped gold tip, respectively.

example, gold domains can be grown selectively on the tips of CdSe or CdS nanorods.[1,32,38−40] These structures have a gold tip either on both ends ("dumbbell" structure) or only at one side ("matchstick" structure). The optical properties of the CdSe−Au and CdS−Au hybrid particles arise from a complex interplay of the components. The rapid electron transfer from the semiconductor to the metal leads to quenching of the fluorescence from the semiconductor part.[1,13] For CdS−Au hybrids, the optical absorption spectra exhibit resonances in the visible and near-UV spectral region that originate from contributions of both the metal (plasmon resonance peak) and the semiconductor (exciton band edge absorption peak). In the NIR range an absorption tail is seen, which falls off toward the IR. Toward higher photon energies, the absorbance of CdS−Au hybrids increases continuously due to excitation of bound electrons into higher bands in both the metal and the semiconductor segments.

It is not straightforward to describe the optical resonances of hybrid structures with plasmonic and excitonic contributions. In fact, the two kinds of excitations have different origins and are normally described by different physical theories since excitons correspond to bound states of a single electron−hole pair,[41] while surface plasmons are collective oscillations of all conduction electrons within the boundaries given by the particle surface.[42] The latter are usually described with classical electrodynamic theory as oscillation of the quasi-free electron cloud within the particle's boundaries.

The interaction between the two kinds of quasiparticles is, in general, highly complex. Here we model this interplay taking into account only purely electrodynamic interaction of otherwise independent systems. In this approach both systems are described by their independent dielectric function, the optical response of the hybrid being then computed numerically within the discrete dipole approximation (DDA).[43,44] We compare theoretical calculations to experimental results based on absorption measurements of hybrid CdS−Au and CdSe−Au nanoparticles corresponding to non-resonant and resonant exciton−plasmon interaction, respectively.

RESULTS AND DISCUSSION

Figure 1a shows a TEM image of the CdS−Au sample for which the optical response was studied (CdS size: 14 nm × 5.3 nm, D_{Au} = 6 nm). Figure 1b shows the measured absorption spectra of the sample before and after gold growth. In this size range, scattering is usually much smaller than absorption, and therefore the latter dominates the optical response. In order to understand the optical resonances seen in the absorption spectrum of this CdS−Au sample in more detail, we have performed electrodynamic simulations within the DDA approximation using the dielectric functions of the confined metal and semiconductor parts as inputs. The geometry used in the calculation is shown in the schematic drawing in Figure 1c. The sizes correspond to the mean dimensions of the prepared sample seen in Figure 1a. The gold tip was described as a sphere with a diameter of D = 6 nm. The length (L) and diameter (w) of the CdS cylinder-shaped segment were set as 14 and 5.3 nm, respectively. Possible deviations of the tip from a perfect spherical shape were taken into account by changing the overlap between the sphere and the cylinder described by the S parameter (see Figure 1c).

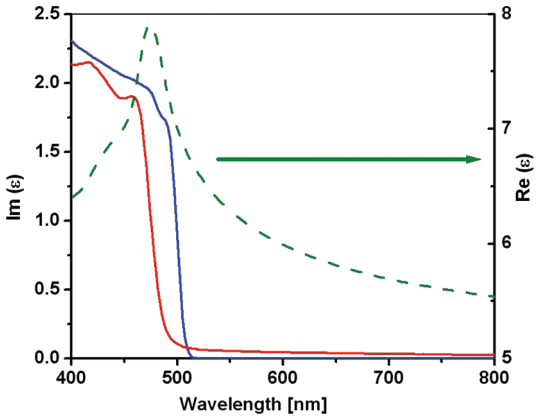

Figure 2. Computed dielectric functions (DEFs): (solid blue curve) imaginary part of the dielectric function of bulk CdS,[45] (solid red curve) imaginary part of the dielectric function of the CdS nanorod sample (16.5 nm × 5.7 nm), (green dashed curve) the real part of the dielectric function of the CdS nanorods sample.

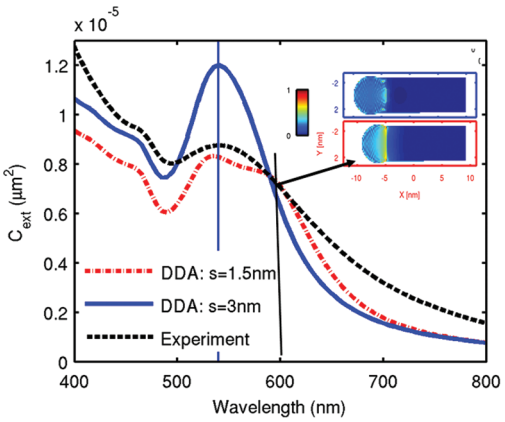

Figure 3. Wavelength-dependent absorption cross section is shown for three cases: experimental spectra obtained from absorption measurements (dashed black line), DDA simulation taking into account half-sphere-shaped gold tip, *S* = 1.5 nm (dashed red line), DDA simulation taking into account a spherical gold tip, *S* = 3 nm (blue line). The simulation for the half-sphere-shaped gold tip exhibits a second plasmon resonance around 600 nm (black vertical line) corresponding to a resonance with the electric field located along the interface (inset: color-coded local polarization when excited with light polarized parallel to the short particle axis).

Describing the response of the metal−semiconductor hybrid structures is complicated because the electron confinement has a strong influence on the dielectric functions (DEF) of the semiconductor part. To obtain it, we started from the experimental absorption spectra of bare semiconductor nanorods of similar sizes to those in the hybrid structures and employed an iterative procedure to systematically improve a trial DEF, which by construction coincided with the bulk CdSe and CdS DEFs above a threshold frequency, until the calculated and experimental absorption spectra coincide.[45] The extracted imaginary part of the dielectric function for the CdS nanorod is shown in Figure 2 (red curve) in comparison to that of bulk CdS (blue curve). The real part of the dielectric function calculated using the Kramers−Krönig relation for the CdS nanorods is also shown (green dashed curve in Figure 2). The procedure for calculating DEFs of the semiconductor is described in detail in the Computational Methods section and in the Supporting Information.

For the size range of the gold part investigated here, size effects on the DEF must be taken into account by modifying the bulk DEF[46] with a size-dependent damping term that takes into account the surface scattering of electrons.[42,47,48] This essentially leads to a broadening of the surface plasmon resonance of metal nanoparticles. In this context, DDA has been widely used to simulate the optical properties of metal nanostructures,[49−51] as it permits calculation for arbitrary shapes. In a previous study,[52] we found good agreement with the measured optical properties of relatively "large" gold nanoparticles using the bulk DEF of gold.

Apart from the size effect on the DEF of the gold, the exact shape of the metal−semiconductor interface and the gold tip shape also play an important role. In order to elucidate their effect on the absorption of the CdS−Au hybrid, we simulated the absorption spectra for two different cases: half-sphere-shaped tip and a spherical tip (*S* = 1.5 nm and *S* = 3 nm, respectively; see drawing in Figure 1c) attached to a semiconductor cylinder. The simulation results are given in Figure 3 in comparison with the experimentally obtained spectra. As the measured spectra are for a dilute solution of nanoparticles dissolved in toluene with a well defined size and shape, we model the nanoparticles as isolated hybrid particles that are not interacting with each other. For the half-sphere, we obtained two plasmon resonances (red curve). The resonance corresponding to the peak around 600 nm, which is not present in the experimental spectra, is associated with an enhanced electric field along the interface (see black vertical line and inset in Figure 3). This resonance also showed up in calculations of half-sphere-shaped gold nanoparticles without any semiconductor part. Therefore, we assume that this extra resonance originated from the edged anisotropic shape of the gold domain within the hybrid nanoparticle. This is also consistent with the slight blue shift of the short wavelength resonance (around 530 nm) as compared to the spherical case. Deviation from sphericity of a pure metal nanoparticle is known to induce a splitting of the surface plasmon resonance into red- and blue-shifted component, as in a metal nanorod.

For the spherical gold domains (Figure 3, blue curve) this second resonance disappears. The simulation obtained for a spherical tip exhibits a single plasmon peak in a location that coincides with the plasmon peak in the measured absorption spectra (Figure 3, black

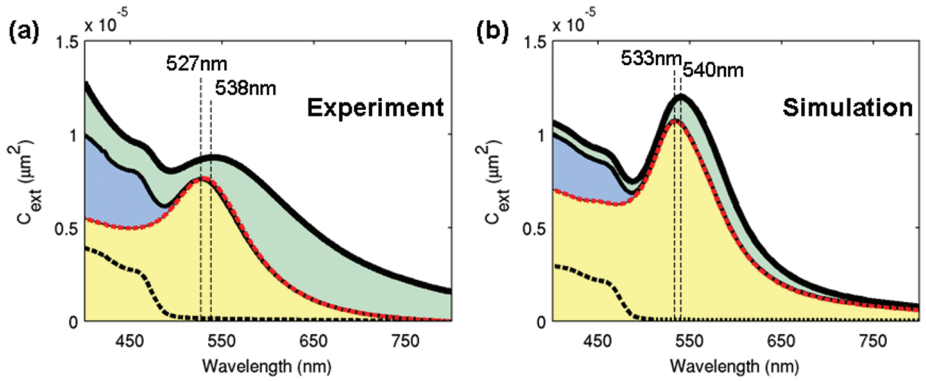

Figure 4. Extinction cross section (in μm^2) as a function of wavelength for 16.5 nm × 5.8 nm bare CdS nanorods (dashed black curve), 6 nm gold bare nanoparticles (red dotted curve and yellow area), a mixture of gold nanoparticles and CdS nanorods with dimensions similar to those in the hybrid (yellow plus blue area, narrow black curve), CdS−Au hybrid (thick black line), and the difference between hybrid *versus* the mixture of its components (green area). For all the spectra the solvent is toluene. We compare the spectra obtained in two different approaches: (a) experimental absorption measurements; (b) DDA simulations. The estimated error for the experimentally obtained absorption cross section of CdS and CdS−Au values is ∼20%.

curve). From this observation we can conclude two things: first, the optical spectra depend very sensitively on small variations of the gold domain shape, and second, it appears that the gold domain in these matchstick-shaped CdS−Au hybrids is best accounted for as a sphere. This analysis clearly demonstrates the remarkable sensitivity of the DDA method to the metal domain shape and to the interface between the two materials. This information is difficult to obtain by direct structural characterization methods such as electron microscopy or by any other means.

Additionally, we compare the absorption spectra of the CdS−Au hybrid with the absorption of a mixture of its individual components. This is aimed to elucidate the influence of combining the two materials together on the absorbance of the hybrid. The comparison was conducted both for experimentally measured absorption spectra in toluene and for theoretical DDA simulations (using toluene as the solvent), as shown in Figure 4a and 4b, respectively.

In both cases, namely, experiment and DDA simulation, we compare the absorption cross section of the CdS−Au hybrid sample (CdS: 14 nm × 5.3 nm, D_{Au} = 6 nm) as a function of wavelength (thick black curve) to the result obtained for a physical mixture of CdS nanorods (16.5 × 5.8 nm) and free gold nanoparticles (D_{Au} = 6 nm) with a mole ratio of 1:1 (narrow black curve, above the yellow and blue areas; the mole amount corresponds to number of particles, *not* atoms). The experimental result was obtained by measuring a mixture of CdS nanorods and gold nanoparticles in toluene and normalizing the absorption spectra of the mixture to the absorption cross section of 6 nm gold nanoparticles. The cross section for the gold was obtained from inductive coupled plasma atomic emission spectroscopy measurements combined with absorbance measurements, as explained in the Supporting Information (C_{ext} at 525 nm = 8 × 10^{-6} μm^2). The DDA result for the mixture is based on the sum of the results obtained separately for bare gold spheres and CdS nanorods. For clarity, we also add to the plots in Figure 4a and 4b the wavelength-dependent absorption cross sections for bare Au nanoparticles (red dashed curve) and bare CdS nanorods (black dashed curve) of similar dimensions to those within the hybrids (see details in the Experimental Methods section and in the Supporting Information).

We find a qualitative agreement between the DDA simulations and the experimental results given in Figure 4. In the experimental spectra, the plasmon peak in the hybrid is red-shifted to lower energies/longer wavelength with respect to the plasmon of the mixture (shifts from 527 to 538 nm, by about 50 meV). A spectral red shift of similar magnitude is observed also in the simulation (from 533 to 540 nm, by about 30 meV). Therefore, it appears that the simulation confirms that this red shift is mainly a purely electrodynamic effect, caused by the larger real part of the refractive index of the semiconductor as compared to that of the solvent surrounding the metal tip. This behavior is consistent with previous observations of plasmon resonance shift toward lower energies (spectral red shift) in a higher refractive index environment.[53,54] However, we point out that in contrast to spherical symmetry systems, *e.g.*, nanospheres in different matrixes or core/shell structures, for these matchstick-shaped CdS−Au hybrids, the surrounding environment of the gold tip is not homogeneous, as the tip is directly exposed to both the semiconductor domain on one side and the solvent on the other side.

In addition, for the experiment and the simulation, the absorption cross section of the hybrid nanoparticles is slightly larger compared to that of the mixture of their components (see green area in Figure 4), again an effect of the larger dielectric constant environment. However, we note that the experimental spectrum of

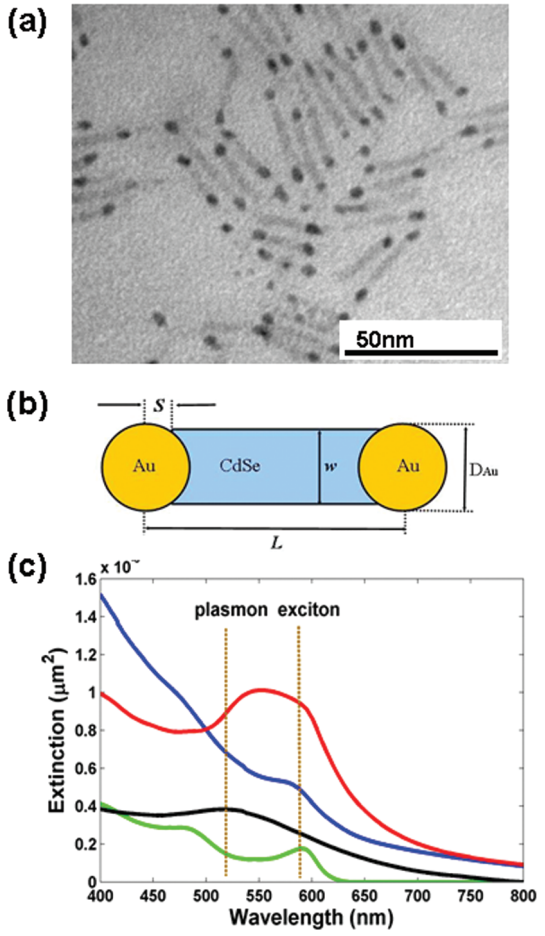

Figure 5. (a) TEM image of the CdSe–Au dumbbell-shaped hybrid sample for which the absorption was studied (CdSe: 24 × 4.4 nm, D_{Au} = 4.4 nm). (b) Schematic drawing of the geometry of the CdSe-Au hybrid used for the DDA simulation. The following values were used for the simulation: D = 4.4 nm, L = 26 nm, w = 4.4 nm, solvent: toluene. (c) Wavelength-dependent absorption cross sections are shown for the CdSe–Au dumbbell-shaped sample. The experimentally obtained spectrum (blue curve) is shown in comparison to the DDA simulation result (red curve). For further comparison, the absorption cross section spectra for bare CdSe nanorods (24 × 4.4 nm, green curve) and bare gold nanoparticles (D_{Au} = 4.4 nm, black curve) are shown (obtained based on absorption measurements in toluene). The locations of the band edge exciton absorption peak of the bare CdSe nanorods and the plasmon resonance peak of the bare gold nanoparticles are marked for clarity (brown dotted line).

the CdS–Au hybrid (Figure 4a) is broader than the DDA simulation spectra (Figure 4b). This could be caused by the inhomogeneous size and shape distribution of the real sample in the experimental ensemble absorption measurements in contrast to the fixed geometry used in the simulations.

Aiming to understand the validity of the introduced theoretical method for the study of other types of semiconductor–metal hybrids, we have also applied the combined experimental and theoretical study to a sample of CdSe–Au dumbbell-shaped nanoparticles. In contrast to the CdS–Au case, in this system the surface plasmon resonance of the bare gold tip overlaps the absorption of the bare semiconductor rod. Figure 5a shows a TEM image of the sample for which the absorption was studied (CdSe: 24 × 4.5 nm, D_{Au} = 4.5 nm). The absorption of the CdSe–Au sample was calculated using the same numerical approach with the geometry shown in Figure 5b. The sizes used in the calculation correspond to the dimensions of the prepared sample seen in Figure 5a. The gold tip was described as a sphere with a diameter of D = 4.4 nm. The length (L) and diameter (w) of the CdSe cylinder-shaped segment were set as 23.8 and 4.4 nm, respectively. The S parameter was set to a value of 1.1 nm. The absorption cross sections were obtained experimentally in the same manner as for CdS–Au hybrids.

Figure 5c shows the absorption spectra obtained for CdSe–Au from the simulation (red curve) in comparison with the experimental result (blue curve). As a reference, we add the spectra obtained for bare CdSe nanorods (green curve) and gold nanoparticles (black curve) of similar sizes (obtained experimentally based on absorption measurements in toluene). The simulation for CdSe–Au predicts the appearance of a broad peak around 570 nm, arising from the absorbance of both components. However, in the experimental spectra, no plasmon resonance peak is seen and the exciton absorption peak is smeared. It appears that for CdSe–Au hybrids, the absorbance is governed by additional effects that cannot be accounted for using only an electrodynamics approach, unlike the case of CdS–Au. This difference can be ascribed to the spectral overlap between the absorbance of the metal domain and that of the semiconductor domain. This leads to strong mixing of the electronic states of the metal and the semiconductor, which may influence the absorption spectrum, an effect that is not accounted for in the simulation.

CONCLUSIONS

Keeping in mind the limitations of the adopted simulation approach, namely, the inclusion of only polarizability effects within the DDA method with the dielectric functions of the confined but non-interacting components, the comparison of single-particle spectra (theory) to ensemble spectra (experiment), and the uncertainty in the gold tip geometry, we can nevertheless use the qualitative agreement between simulation and experiment for CdS–Au "matchstick" hybrids to draw conclusions. In this non-resonant condition between the semiconductor and metal excitations, the sensitivity of the DDA method to the metal tip shape combined with experimental results provides important insights on the shape of the gold tip and the interface for the CdS–Au hybrids. Such structural characterization is difficult to acquire by experimental means alone.

Furthermore, the qualitative agreement between DDA simulation and experiment for CdS–Au shows that most effects influencing the absorption of

CdS–Au hybrid nanoparticles are reasonably well captured by local dielectric functions obtained from the spectra of the bare nanoparticles. In such a case, the contact between the two materials seems to have only a secondary effect on the dielectric function of the hybrid, *i.e.*, their electronic band structure.

Nevertheless, we point out that the optical features we investigated are rather broad, and the simulations contain some free parameters (mainly the exact geometry of the gold tips) that render the latter conclusion preliminary. Furthermore, our study shows that taking into account only polarizability effects is not sufficient to describe all types of hybrid systems, especially in a strong interaction case of CdSe–Au hybrids. Our current approach, which relies primarily on the dielectric functions of the component comprising the hybrid, does not take into account additional effects that may influence the absorption such as the creation of coupled modes, modification of the electronic structure of the materials, charge transfer between the domains, or crystal strains due to lattice mismatch between adjacent domains within the hybrid nanoparticle.

The synthesis and basic optical properties of various semiconductor–metal hybrid systems have been extensively studied in recent years. However, to date, many of the experimental observations are not accounted for by theory. The description of the optical properties of these hybrids remains a challenge. The combined experimental and theoretical study of absorption of CdS–Au nanoparticles described in this paper serves as a first-level treatment of this important and complex problem. We approach this problem by utilizing methods used to describe the absorption properties of semiconductors and metal nanoparticles separately, aiming at the qualitative behavior of the hybrid system represented in a simplified manner as a sum over the components. It is straightforward to expand this to include size distribution effects and an anisotropy of the DEFs, but these are, in our opinion, not the most interesting and important aspects. Future studies need to extend from this point, to address the above mentioned limitations. The most important aspect that challenges current theoretical approaches is to incorporate the electronic interaction of the metal and semiconductor portions of the hybrid system and model the resulting modifications to the DEFs. Inclusion of this aspect is particularly needed for representing systems where the semiconductor exciton and metal plasmon are in resonance, such as in the CdSe–Au system.

EXPERIMENTAL AND COMPUTATIONAL METHODS

Discrete Dipole Approximation Simulations. The DDA method discretizes the hybrid nanoparticles into small boxes, each with a local optical response given by a frequency-dependent dielectric function (DEF). On the basis of these, the overall extinction cross section can be calculated.[43,44] The advantage of this method is that one is completely flexible in choosing the geometry and composition of the structure; however, this comes at the expense of considerable demand on computational power and memory usage. The dielectric functions are, in general, functions of crystal direction and wave vector, but for most applications (also in this study), they are approximated by isotropic functions only depending on frequency.

We generate the dipole models for the DDA calculation using Matlab scripts with a minimum of 30 dipoles per direction. The numerical evaluation is done using the ADDA software package.[55] For the illumination we assume plane waves with a polarization either parallel or perpendicular to the long axis of the nanorod and average over all possible particle orientations by taking a weighted sum of the spectra for the two orthogonal polarization directions. The wavelength resolution is set to 5 nm, and the refractive index of the surrounding medium is chosen to be $n = 1.5$, corresponding to toluene.

Calculations of Dielectric Functions of Semiconductor Nanorods. We determine the dielectric function of a semiconductor nanorod by means of an iterative procedure,[45] which starts from the experimental absorption spectrum of a sample of nanorods with the desired sizes and a trial DEF, which is improved until the corresponding nanoparticle theoretical spectrum matches the experimental one. The computational scheme used here extends the method proposed in our earlier study[45] by using the separation of variables method (SVM)[56] to calculate the extinction cross section of ellipsoidal particles. In this way, a nanorod with diameter D and length L is approximated by an ellipsoid of main axes a and b, chosen to fix $a/b = D/L$ and the ellipsoid volume equal to the target nanorod volume. Within the calculation procedure, the limitation on the energy range available from typical experimental absorption spectra is overcome by matching exactly the imaginary part $\varepsilon_2(E)$ of the nanorod DEF with the imaginary part $\varepsilon_2^{bulk}(E)$ of the bulk at high energies beyond the experimental range and by assuming there is no electromagnetic energy absorbed below the measured absorption edge. Thus, using the Kramers–Krönig relations that link the real and imaginary parts of the DEF and calculating the nanoparticle extinction spectrum within the measurement energy range, it is possible to extract the complete dielectric function of the nanorod as a function of the energy. Further details on this method are given in the Supporting Information.

Experimental Determination of Absorption Cross Sections for Semiconductor Nanorods, Gold Nanoparticles, and Metal–Semiconductor Hybrids. The molar absorption coefficients for the CdS nanorods were determined based on absorption measurements. For this purpose the absorption coefficient far above the band gap, at 350 nm (3.54 eV), was calculated assuming a bulk-like volume-dependent absorption, as exemplified in a previous study for CdSe nanorods.[57] The molar absorption coefficient per unit volume was calculated from the optical constants of the bulk semiconductor and the solvent based on Maxwell–Garnett theory.[58,59] This calculation was based on previous studies on semiconductor nanocrystals,[60] using the values for the complex refractive index of bulk hexagonal CdS ($n = 2.58 + 0.47i$)[61] and toluene ($n = 1.5$) at 350 nm (see further details in the Supporting Information). From the calculation, a value of ε_{350} ($cm^{-1}\ M^{-1}$) = $(0.28 \times 10^{26})V$ (where V is the nanocrystal volume in cm^3) was obtained for CdS nanocrystals. The absorption coefficient of the nanorods at the exciton peak (around 470 nm) was obtained from ε_{350} and the ratio between the measured absorption (OD) at 350 nm and 470 nm as follows:

$$\varepsilon_{470nm} = \varepsilon_{350nm}\frac{OD_{470nm}}{OD_{350nm}} \quad (1)$$

The absorption coefficients for hybrid metal−semiconductor nanoparticles were obtained directly from absorbance measurements by comparing the absorption of the bare semiconductor template to the absorption of the same sample immediately after gold growth solution was added and gold growth has taken place (see Figure 1b). This calculation is based on the homogeneous growth of gold on all the nanocrystals in the sample and on the fact that the number of nanocrystals in the solution did not change during the reaction. The following equation was used to determine the molar absorption coefficient (ε) value at the wavelength of the first exciton absorption peak of the semiconductor segment:

$$\varepsilon_{\text{hybrid}} = \frac{\text{OD}_{\text{hybrid}}}{\text{OD}_{\text{semiconductor}}} \frac{V_f}{V_i} \varepsilon_{\text{semiconductor}} \quad (2)$$

$\text{OD}_{\text{semiconductor}}$ and $\text{OD}_{\text{hybrid}}$ are the absorbance values of the solution before and after gold growth, respectively. V_i and V_f are the volume of the solution before and after gold growth solution addition, and $\varepsilon_{\text{semiconductor}}$ is the molar absorption coefficient of the semiconductor template at the exciton peak absorption (typically located at 580−600 nm for CdSe and 460−470 nm for CdS nanorods used in this study). The estimated error for the determined absorption coefficient values is about 20%, evaluated based on the size distribution of the length and diameter of the semiconductor nanorods.

The molar absorption coefficients (ε) of free gold nanoparticles were determined based on a combination of UV−vis absorption measurements and the determination of the concentration of the nanoparticles by inductive coupled plasma atomic emission spectroscopy (ICP-AES). The molar absorption coefficient was determined by plotting the absorbance as function of the concentration. This plot was fit linearly, and the ε value was obtained from the slope based on Beer's law. A detailed description of the ICP measurements procedure is given in the Supporting Information.

The experimentally obtained absorption coefficients (ε, in units of $\text{cm}^{-1}\,\text{M}^{-1}$) were converted to absorption cross sections (C_{ext}, in units of cm^2) based on the following equation:

$$C_{\text{ext}} = \frac{2303\varepsilon_{\text{abs}}}{N_A} \quad (3)$$

where N_A is the Avogadro constant.

Acknowledgment. We acknowledge financial support by the European Union through the NanoSci ERA-Net scheme under the program single-nanoHybrid. Simulations were performed on the central university cluster of the University of Mainz. We thank Yigal Erel and Ofir Tirosh from the Institute of Earth Science at The Hebrew University for their technical assistance with ICP-AES measurements. U.B. thanks the Alfred & Erica Larisch Memorial chair. G.G. and R.D.F. thank Ulrich Hohenester and Andreas Truegler for fruitful discussions and Garima Jaithliya for technical aspects on the DDA grids in the early stages of this work.

Supporting Information Available: Convergence tests for DDA; calculations of dielectric functions of CdS and CdSe nanorods; preparation of metal−semiconductor samples; experimental determination of absorption cross sections of CdS nanorods; determination of molar absorption coefficients for gold nanoparticles. This material is available free of charge *via* the Internet at http://pubs.acs.org.

REFERENCES AND NOTES

1. Mokari, T.; Rothenberg, E.; Popov, I.; Costi, R.; Banin, U. Selective Growth of Metal Tips onto Semiconductor Quantum Rods and Tetrapods. *Science* **2004**, *304*, 1787–1790.
2. Cozzoli, P. D.; Pellegrino, T.; Manna, L. Synthesis, Properties and Perspectives of Hybrid Nanocrystal Structures. *Chem. Soc. Rev.* **2006**, *35*, 1195–1208.
3. Costi, R.; Saunders, A. E.; Banin, U. Colloidal Hybrid Nanostructures: A New Type of Functional Materials. *Ang. Chem., Int. Ed.* **2010**, *49*, 4878–4897.
4. Carbone, L.; Cozzoli, P. D. Colloidal Heterostructured Nanocrystals: Synthesis and Growth Mechanisms. *Nano Today* **2010**, *5*, 449–493.
5. Cortie, M. B.; McDonagh, A. M. Synthesis and Optical Properties of Hybrid and Alloy Plasmonic Nanoparticles. *Chem. Rev.* 2011 [Online early access] DOI:10.1021/cr1002529. Published online: Jan 14, 2011. http://pubs.acs.org/journal/chreay (accessed March 15, 2011).
6. Peng, X.; Schlamp, M. C.; Kadavanich, A. V.; Alivisatos, A. P. Epitaxial Growth of Highly Luminescent CdSe/CdS Core/Shell Nanocrystals with Photostability and Electronic Accessibility. *J. Am. Chem. Soc.* **1997**, *119*, 7019–7029.
7. Halpert, J. E.; Porter, V. J.; Zimmer, J. P.; Bawendi, M. G. Synthesis of CdSe/CdTe Nanobarbells. *J. Am. Chem. Soc.* **2006**, *128*, 12590–12591.
8. Shieh, F.; Saunders, A. E.; Korgel, B. A. General Shape Control of Colloidal CdS, CdSe, CdTe Quantum Rods and Quantum Rod Heterostructures. *J. Phys. Chem. B* **2005**, *109*, 8538–8542.
9. Milliron, D. J.; Hughes, S. M.; Cui, Y.; Manna, L.; Li, J. B.; Wang, L. W.; Alivisatos, A. P. Colloidal Nanocrystal Heterostructures with Linear and Branched Topology. *Nature* **2004**, *430*, 190–195.
10. Buonsanti, R.; Grillo, V.; Carlino, E.; Giannini, C.; Curri, M. L.; Innocenti, C.; Sangregorio, C.; Achterhold, K.; Parak, F. G.; Agostiano, A.; *et al.* Seeded Growth of Asymmetric Binary Nanocrystals Made of a Semiconductor TiO_2 Rodlike Section and a Magnetic y-Fe_2O_3 Spherical Domain. *J. Am. Chem. Soc.* **2006**, *128*, 16953.
11. Casavola, M.; Grillo, V.; Carlino, E.; Giannini, C.; Gozzo, F.; Fernandez Pinel, E.; Garcia, M. A.; Manna, L.; Cingolani, R.; Cozzoli, P. D. Topologically Controlled Growth of Magnetic-Metal-Functionalized Semiconductor Oxide Nanorods. *Nano Lett.* **2007**, *7*, 1386–1395.
12. Pacholski, C.; Kornowski, A.; Weller, H. Site-Specific Photodeposition of Silver on ZnO Nanorods. *Ang. Chem., Int. Ed.* **2004**, *43*, 4774–4777.
13. Saunders, A. E.; Popov, I.; Banin, U. Synthesis of Hybrid CdS-Au Colloidal Nanostructures. *J. Phys. Chem. B* **2006**, *110*, 25421–25429.
14. Cozzoli, P. D.; Curri, M. L.; Giannini, C.; Agostiano, A. Synthesis of TiO_2-Au Composites by Titania-Nanorod-Assisted Generation of Gold Nanoparticles at Aqueous/Nonpolar Interfaces. *Small* **2006**, *2*, 413–421.
15. Carbone, L.; Kudera, S.; Giannini, C.; Ciccarella, G.; Cingolani, R.; Cozzoli, P. D.; Manna, L. Selective Reactions on the Tips of Colloidal Semiconductor Nanorods. *J. Mater. Chem.* **2006**, *16*, 3952–3956.
16. Liu, H.; Alivisatos, A. P. Preparation of Asymmetric Nanostructures through Site Selective Modification of Tetrapods. *Nano Lett.* **2004**, *4*, 2397–2401.
17. Khalavka, Y.; Sönnichsen, C. Growth of Gold Tips onto Hyperbranched CdTe Nanostructures. *Adv. Mater.* **2008**, *20*, 588.
18. Kamat, P. V. Quantum Dot Solar Cells. Semiconductor Nanocrystals as Light Harvesters. *J. Phys. Chem. C* **2008**, *112*, 18737–18753.
19. Subramanian, V.; Wolf, E. E.; Kamat, P. V. Catalysis with TiO_2/Gold Nanocomposites. Effect of Metal Particle Size on the Fermi Level Equilibration. *J. Am. Chem. Soc.* **2004**, *126*, 4943–4950.
20. Shemesh, Y.; Macdonald, J. E.; Menagen, G.; Banin, U. Synthesis and Photocatalytic Properties of a Family of CdS-PdX Hybrid Nanoparticles. *Ang. Chem., Int. Ed.* **2011**, *50*, 1185–1189.
21. Sheldon, M. T.; Trudeau, P. E.; Mokari, T.; Wang, L. W.; Alivisatos, A. P. Enhanced Semiconductor Nanocrystal Conductance via Solution Grown Contacts. *Nano Lett.* **2009**, *9*, 3676–3682.
22. Alivisatos, A. P. Perspectives on the Physical Chemistry of Semiconductor Nanocrystals. *J. Phys. Chem.* **1996**, *100*, 13226–13239.
23. Eustis, S.; El-Sayed, M. A. Why Gold Nanoparticles are More Precious Than Pretty Gold: Noble Metal Surface Plasmon Resonance and its Enhancement of the Radiative and

Nonradiative Properties of Nanocrystals of Different Shapes. *Chem. Soc. Rev.* **2006**, *35*, 209–217.
24. Lin, H. Y.; Chen, Y. F.; Wu, J. G.; Wang, D. I.; Chen, C. C. Carrier Transfer Induced Photoluminescence Change in Metal-Semiconductor Core-Shell Nanostructures. *Appl. Phys. Lett.* **2006**, 88.
25. Fedutik, Y.; Temnov, V.; Woggon, U.; Ustinovich, E.; Artemyev, M. Exciton-Plasmon Interaction in a Composite Metal-Insulator-Semiconductor Nanowire System. *J. Am. Chem. Soc.* **2007**, *129*, 14939–14945.
26. Shimizu, K. T.; Woo, W. K.; Fisher, B. R.; Eisler, H. J.; Bawendi, M. G. Surface-Enhanced Emission from Single Semiconductor Nanocrystals. *Phys. Rev. Lett.* **2002**, *89*, 117401.
27. Lee, J.; Govorov, A. O.; Dulka, J.; Kotov, N. A. Bioconjugates of CdTe Nanowires and Au Nanoparticles: Plasmon-Exciton Interactions, Luminescence Enhancement, and Collective Effects. *Nano Lett.* **2004**, *4*, 2323–2330.
28. Zhang, W.; Govorov, A. O.; Bryant, G. W. Semiconductor-Metal Nanoparticle Molecules: Hybrid Excitons and the Nonlinear Fano Effect. *Phys. Rev. Lett.* **2006**, 97.
29. Mulvaney, P. Surface Plasmon Spectroscopy of Nanosized Metal Particles. *Langmuir* **1996**, *12*, 788–800.
30. Hirakawa, T.; Kamat, P. V. Photoinduced Electron Storage and Surface Plasmon Modulation in Ag@TiO_2 Clusters. *Langmuir* **2004**, *20*, 5645–5647.
31. Wood, A.; Giersig, M.; Mulvaney, P. Fermi Level Equilibration in Quantum Dot-Metal Nanojunctions. *J. Phys. Chem. B* **2001**, *105*, 8810–8815.
32. Carbone, L.; Jakab, A.; Khalavka, Y.; Sonnichsen, C. Light-Controlled One-Sided Growth of Large Plasmonic Gold Domains on Quantum Rods Observed on the Single Particle Level. *Nano Lett.* **2009**, *9*, 3710–3714.
33. Costi, R.; Saunders, A. E.; Elmalem, E.; Salant, A.; Banin, U. Visible Light-Induced Charge Retention and Photocatalysis with Hybrid CdSe-Au Nanodumbbells. *Nano Lett.* **2008**, *8*, 637–641.
34. Elmalem, E.; Saunders, A. E.; Costi, R.; Salant, A.; Banin, U. Growth of Photocatalytic CdSe-Pt Nanorods and Nanonets. *Adv. Mater.* **2008**, *20*, 4312–4317.
35. Cozzoli, P. D.; Curri, M. L.; Agostiano, A. Efficient Charge Storage in Photoexcited TiO_2 Nanorod-Noble Metal Nanoparticle Composite Systems. *Chem. Commun.* **2005**, 3186–3188.
36. Figuerola, A.; Franchini, I. R.; Fiore, A.; Mastria, R.; Falqui, A.; Bertoni, G.; Bals, S.; Van Tendeloo, G.; Kudera, S.; Cingolani, R.; *et al.* End-to-End Assembly of Shape-Controlled Nanocrystals via a Nanowelding Approach Mediated by Gold Domains. *Adv. Mater.* **2009**, *21*, 550–554.
37. Salant, A.; Amitay-Sadovsky, E.; Banin, U. Directed Self-Assembly of Gold-Tipped CdSe Nanorods. *J. Am. Chem. Soc.* **2006**, *128*, 10006–10007.
38. Menagen, G.; Macdonald, J. E.; Shemesh, Y.; Popov, I.; Banin, U. Au Growth on Semiconductor Nanorods: Photoinduced versus Thermal Growth Mechanisms. *J. Am. Chem. Soc.* **2009**, *131*, 17406–17411.
39. Mokari, T.; Sztrum, C. G.; Salant, A.; Rabani, E.; Banin, U. Formation of Asymmetric One-Sided Metal-Tipped Semiconductor Nanocrystal Dots and Rods. *Nat. Mater.* **2005**, *4*, 855–863.
40. Figuerola, A.; Huis, M. v.; Zanella, M.; Genovese, A.; Marras, S.; Falqui, A.; Zandbergen, H. W.; Cingolani, R.; Manna, L. Epitaxial CdSe-Au Nanocrystal Heterostructures by Thermal Annealing. *Nano Lett.* **2010**, *10*, 3028–3036.
41. Yu, P. Y.; Cardona, M. *Fundamentals of Semiconductors: Physics and Materials Properties*, 4th ed.; Springer: Berlin, 2010; p 276.
42. Link, S.; Ei-Sayed, M. A. Optical Properties and Ultrafast Dynamics of Metallic Nanocrystals. *Annu. Rev. Phys. Chem.* **2003**, *54*, 331–366.
43. Myroshnychenko, V.; Rodriguez-Fernandez, J.; Pastoriza-Santos, I.; Funston, A. M.; Novo, C.; Mulvaney, P.; Liz-Marzan, L. M.; de Abajo, F. J. G. Modelling the Optical Response of Gold Nanoparticles. *Chem. Soc. Rev.* **2008**, *37*, 1792–1805.
44. Zhao, J.; Pinchuk, A. O.; McMahon, J. M.; Li, S. Z.; Ausman, L. K.; Atkinson, A. L.; Schatz, G. C. Methods for Describing the Electromagnetic Properties of Silver and Gold Nanoparticles. *Acc. Chem. Res.* **2008**, *41*, 1710–1720.
45. Alves-Santos, M.; Di Felice, R.; Goldoni, G. Dielectric Functions of Semiconductor Nanoparticles from the Optical Absorption Spectrum: The Case of CdSe and CdS. *J. Phys. Chem. C* **2010**, *114*, 3776–3780.
46. Johnson, P. B.; Christy, R. W. Optical Constants of the Noble Metals. *Phys. Rev. B* **1972**, *6*, 4370–4379.
47. Kreibig, U.; Genzel, L. Optical-Absorption of Small Metallic Particles. *Surf. Sci.* **1985**, *156*, 678–700.
48. Baida, H.; Billaud, P.; Marhaba, S.; Christofilos, D.; Cottancin, E.; Crut, A.; Lerme, J.; Maioli, P.; Pellarin, M.; Broyer, M.; *et al.* Quantitative Determination of the Size Dependence of Surface Plasmon Resonance Damping in Single Ag@SiO_2 Nanoparticles. *Nano Lett.* **2009**, *9*, 3463–3469.
49. Yang, W. H.; Schatz, G. C.; Vanduyne, R. P. Discrete Dipole Approximation for Calculating Extinction and Raman Intensities for Small Particles with Arbitrary Shapes. *J. Chem. Phys.* **1995**, *103*, 869–875.
50. Schatz, G. C. Electrodynamics of Nonspherical Noble Metal Nanoparticles and Nanoparticle Aggregates. *J. Mol. Struct. (Theochem)* **2001**, *573*, 73–80.
51. Muskens, O. L.; Bachelier, G.; Del Fatti, N.; Vallee, F.; Brioude, A.; Jiang, X. C.; Pileni, M. P. Quantitative Absorption Spectroscopy of a Single Gold Nanorod. *J. Phys. Chem. C* **2008**, *112*, 8917–8921.
52. Schubert, O.; Becker, J.; Carbone, L.; Khalavka, Y.; Provalska, T.; Zins, I.; Sonnichsen, C. Mapping the Polarization Pattern of Plasmon Modes Reveals Nanoparticle Symmetry. *Nano Lett.* **2008**, *8*, 2345–2350.
53. Sönnichsen, C.; Geier, S.; Hecker, N. E.; von Plessen, G.; Feldmann, J.; Ditlbacher, H.; Lamprecht, B.; Krenn, J. R.; Aussenegg, F. R.; Chan, V. Z. H.; *et al.* Spectroscopy of Single Metallic Nanoparticles using Total Internal Reflection Microscopy. *Appl. Phys. Lett.* **2000**, *77*, 2949–2951.
54. Templeton, A. C.; Pietron, J. J.; Murray, R. W.; Mulvaney, P. Solvent Refractive Index and Core Charge Influences on the Surface Plasmon Absorbance of Alkanethiolate Monolayer-Protected Gold Clusters. *J. Phys. Chem. B* **2000**, *104*, 564–570.
55. Hoekstra, A. G.; Grimminck, M. D.; Sloot, P. M. A. Large Scale Simulations of Elastic Light Scattering by a Fast Discrete Dipole Approximation. *Int. J. Mod. Phys. C* **1998**, *9*, 87–102.
56. Voshchinnikov, N. V.; Farafonov, V. G. Optical-Properties of Spheroidal Particles. *Astrophys. Space Sci.* **1993**, *204* 19–86.
57. Shaviv, E.; Salant, A.; Banin, U. Size Dependence of Molar Absorption Coefficients of CdSe Semiconductor Quantum Rods. *ChemPhysChem* **2009**, *10*, 1028–1031.
58. Maxwell-Granett, J. C. Colours in Metal Glasses and in Metallic Films. *Philos. Trans. R. Soc. London A* **1904**, *203*, 385–420.
59. Sihvola, A. Two Main Avenues Leading to the Maxwell Garnett Mixing Rule. *J. Electromagn. Waves Appl.* **2001**, *15*, 715–725.
60. Leatherdale, C. A.; Woo, W. K.; Mikulec, F. V.; Bawendi, M. G. On the Absorption Cross Section of CdSe Nanocrystal Quantum Dots. *J. Phys. Chem. B* **2002**, *106*, 7619–7622.
61. Palik, E. D. *Handbook of Optical Constants of Solids*, 1st ed.; Academic Press: Orlando, 1985; pp 579−596.